ACS APPLIED MATERIALS & INTERFACES

Research Article

www.acsami.org

Ordered to Isotropic Morphology Transition in Pattern-Directed Dewetting of Polymer Thin Films on Substrates with Different Feature Heights

Sudeshna Roy and Rabibrata Mukherjee*

Department of Chemical Engineering, Indian Institute of Technology−Kharagpur, West Bengal, 721 302, India

Supporting Information

ABSTRACT: Controlled dewetting of a thin polymer film on a topographically patterned substrate is an interesting approach for aligning isotropic dewetted structures. In this article, we investigate the influence of substrate feature height ($\mathbf{H_S}$) on the dewetting pathway and final pattern morphology by studying the dewetting of polystyrene (PS) thin films on grating substrates with identical periodicity (λ_P = 1.5 μm), but $\mathbf{H_S}$ varying between 10 nm and 120 nm. We identify four distinct categories of final dewetted morphology, with different extent of ordering: (1) array of aligned droplets ($\mathbf{H_S} \approx$ 120 nm); (2) aligned undulating ribbons ($\mathbf{H_S} \approx$ 70−100 nm); (3) multilength scale structures with coexisting large droplets uncorrelated to the substrate and smaller droplets/ribbons aligned along the stripes ($\mathbf{H_S} \approx$ 40−60 nm); and (4) large droplets completely uncorrelated to the substrate ($\mathbf{H_S}$ < 25 nm). The distinct morphologies across the categories are attributed to two major factors: (a) whether the as-cast film is continuous ($\mathbf{H_S} \leq$ 80 nm) or discontinuous ($\mathbf{H_S} \geq$ 100 nm) and (b) in case of a continuous film, whether the film ruptures along each substrate stripe ($\mathbf{H_S} \geq$ 70 nm) or with nucleation of random holes that are not correlated to the substrate features ($\mathbf{H_S} \leq$ 60 nm). While the ranges of $\mathbf{H_S}$ values indicated in the parentheses are valid for PS films with an equivalent thickness ($\mathbf{h_E}$) ≈ 50.3 nm on a flat substrate, a change in $\mathbf{h_E}$ merely alters the cut-off values of $\mathbf{H_S}$, as the final dewetted morphologies and transition across categories remain generically unaltered. We finally show that the structures obtained by dewetting on different $\mathbf{H_S}$ substrates exhibits different levels of hydrophobicity because of combined spatial variation of chemical and topographic contrast along the surface. Thus, the work reported in this article can find potential application in fabricating surfaces with controlled wettability.

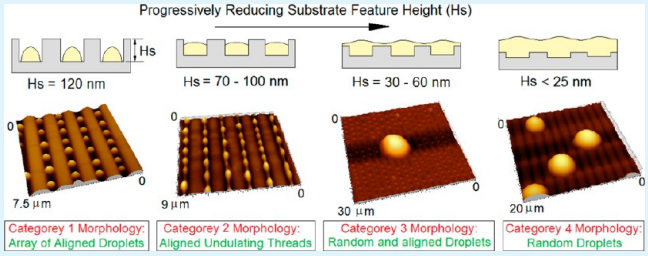

KEYWORDS: *pattern directed dewetting, self organization, meso patterns, thin films, instability*

INTRODUCTION

Spontaneous or nucleated instability and dewetting of an ultrathin polymer film on a solid substrate is a fascinating problem that is important in many practical settings. In coating applications, the integrity of the film is essential and, therefore, strategies are being worked out to suppress any form of instability,[1,2] which requires a thorough understanding of the process itself.[3−10] On the other hand, the morphological self-organization during dewetting is a potential nonlithographic technique for the fabrication of mesoscale and nanoscale surface structures spanning over large areas,[11] which has already been used to fabricate high-density data storage,[12] polymer field-effect transistors,[13,14] optical memory,[15] etc. The onset of instability in a defect-free flat film on a smooth surface occurs with the formation of random, isolated holes. The holes are typically surrounded by a distinct rim that results from a mismatch between the rates at which polymer is dislodged from the substrate and gets redistributed to other intact parts of the film.[4,5,7−10] With time, the holes grow and the rims of the neighboring ones merge with each other, forming a polygonal network of polymer ribbons, resembling the cellular-shaped Voronoi tessellation patterns. The ribbons subsequently break up due to Rayleigh instability, to form isolated droplets aligned along the sides of the polygons. In the event there is an instability in the rim itself during hole growth, the polygonal network formation is suppressed and a completely isotropic array of nearly equal-sized droplets result, which is more pronounced in high-molecular-weight films on low wettability substrates.[5] The morphological evolution sequence, which takes place only when the polymer is heated beyond its glass-transition temperature ($\mathbf{T_G}$), can be stopped at any intermediate stage by quenching the film to a lower temperature (below $\mathbf{T_G}$), which makes it possible to create morphologically distinct structures, such as holes, ribbons, droplets, etc. The instability mediated structures are generally isotropic and the lack of order severely limits their practical utility. In order to utilize dewetting mediated structure formation as a viable patterning technique, it becomes necessary to impose certain degree of order to the dewetted features, a problem that has

Received: July 12, 2012
Accepted: September 21, 2012
Published: September 21, 2012

   dx.doi.org/10.1021/am301311d | *ACS Appl. Mater. Interfaces* 2012, 4, 5375−5385

received significant research attention, both theoretically[16−22] and experimentally.[23−49] While prepatterning a film by rubbing in a specific direction was used to demonstrate the concept for the first time,[23] dewetting on chemically[16,18−21,26−34] and topographically patterned substrates[17,22,35−43] are preferred routes to create aligned patterns in a reproducible manner over large areas. Vertically confining the film under a mold during dewetting has also been utilized to obtain ordered structures.[44−49]

On a chemically patterned substrate comprising of alternating zones of different wettability, dewetting is engendered by the in-plane wettability gradient between the less- and more-wettable areas on the substrate.[16−19] This is in contrast to spinodal dewetting of a film on a homogeneous nonwettable substrate, where dewetting is engendered due to amplification of thermally excited capillary wave spectrum on the film surface, as a result of attractive interfacial van der Waals interaction. Theoretical[16−21] as well as experimental studies[26−35] have identified conditions under which variety of ordered structures can be obtained on a chemically patterned substrate.[16,19,26,27,29−34] Sehgal et al. have shown that a variety of ordered and partially ordered structures are possible, depending on the commensuration between the pattern dimensions (λ_P) and the characteristic length scale of the dewetted features on a flat substrate (λ_D).[29] They have also shown that the ordering tends to get distorted in overconfined systems, where $\lambda_P < \lambda_D$ as the final droplets become anisotropic and coarsen to a scale comparable to the stripe width, eventually transforming into circular droplets leading to quantization droplet size, spanning across multiple stripes.[29] Julthongpiput et al. have shown that there is strong influence of the magnitude of the surface energy gradient ($\Delta\gamma$) between the different wettability domains, as the dewetted patterns transform from highly ordered for high $\Delta\gamma$ to completely isotropic when $\Delta\gamma$ is low, through a crossover regime which bears a combined signature of both isotropic and ordered patterns for intermediate $\Delta\gamma$.[30]

Variety of ordered structures have also been obtained by dewetting polymer thin films on topographically patterned substrates, with different geometry.[36−43] It is seen that, on a grating patterned substrate, the dewetted droplet size and periodicity progressively reduce with a higher degree of lateral confinement, in the form of narrower stripes.[40] In contrast, on a substrate with two-dimensional (2-D) patterns comprising array of square pillars, a perfectly filled and ordered structure is obtained only for a very narrow film thickness range, depending on the commensuration between λ_P and λ_D.[42] It is also possible to obtain aligned structures during spin coating itself, particularly at low concentration of the dispensed polymer solution, which is referred to as spin dewetting.[39,43,50,51]

One of us investigated, in detail, the precise role of substrate topography on dewetting of a film with uniform thickness in an overconfined system, where λ_P is more than an order of magnitude smaller than the length scale of instability of a PS film of same thickness on a flat substrate.[40,42] While the influences of parameters such as pattern geometry, periodicity (λ_P), film thickness (h), etc. has already been investigated,[36−38,40,42] the influence of substrate feature height (H_S) on dewetting of a thin polymer film on a topographically patterned substrate has never been explored before. It is an important parameter as the dewetting morphology becomes isotropic in the limit of a vanishing feature height ($H_S \rightarrow 0$), which corresponds to a homogeneous substrate. Based on thermal dewetting of thin PS films directly spin coated on grating substrates having identical λ_P and different H_S, we report here, for the first time, how both dewetting pathways as well as the final morphology gets influenced by the magnitude of H_S, in topographic pattern-directed dewetting. We identify the existence of four clearly distinct morphological regimes of final dewetted patterns, as a function of H_S. *Category 1* morphology is comprised of tiny dewetted droplets aligned along each substrate stripe, which is observed for the highest values of H_S. The morphology transforms to undulating polymer strips aligned along the substrate grooves with reduction of H_S, which is termed as the *Category 2* morphology. *Category 3* and *Category 4* morphologies are observed for progressively lower H_S, which involve large dewetted droplets, uncorrelated to the substrate stripes resulting due to rupture of the film by nucleation of random holes in a manner similar to that observed on a flat substrate. The only difference between the *Category 3* and *Category 4* morphologies is the existence of tiny droplets aligned along the substrate stripes (similar to *Category 1*), in addition to the large drops in *Category 3*, which are absent in *Category 4*. The distinction in morphology is attributed to a change in the nature of contact line dynamics across these two categories, which again is influenced by H_S. Our investigations also reveal that the initial morphology of the directly spin-coated film on the patterned substrate, particularly whether the film is discontinuous or continuous,[50] has a strong influence on the dewetting sequence and final morphology of the dewetted patterns. We also show that, with change in the effective thickness of the film, the generic morphological categories remain the same, as the cut-off values of H_S between different regimes merely gets altered.

Finally, we show that the different categories of dewetted structures with different extent of ordering exhibits distinct levels of hydrophobicity. We observe that the equilibrium contact angle of water ($\theta_{W\text{-}D}$) on the dewetted surfaces exceeds that observed on a bare patterned cross-linked PDMS substrate ($\theta_{W\text{-}PDMS}$), as well as on a continuous PS film ($\theta_{W\text{-}PS}$) coated on the substrate, because of the combined influence of roughness and chemical contrast generated as a result of dewetting. Thus, dewetting of thin polymer films on substrates with different H_S can find application in fabricating surfaces with tailored hydrophobicity. We also discuss few other potential applications where the findings reported in this article might be useful.

EXPERIMENTAL DETAILS

Patterned cross-linked PDMS (commercially available two-part cross-linkable polydimethylsiloxane (PDMS); Dow Corning, USA) films with grating geometry having a periodicity (λ_P) of 1.5 μm and eight different feature heights (H_S = 120, 100, 80, 70, 60, 40, 25, and 15 nm) were used as substrates in our experiments. In this article, we use the following nomenclature to identify a substrate with a specific feature height: a substrate with a feature height of 120 nm will be identified as a H_{S120} substrate. Similarly, a substrate with a feature height of H_S = 70 nm will be identified as a H_{S70} substrate. The Sylgard 184 film was spin-coated onto 15 mm × 15 mm square pieces of single-side polished silicon wafers (test grade, Wafer World, USA) from its solution in *n*-hexane (SRL, India), and these were patterned by imprinting[52] using lithographically fabricated silicon masters. The thickness of the Sylgard layer was ∼5 μm in all cases, and the ratio of part A to part B was maintained at 10:1 (v/v). After molding, the films, in conformal contact with the stamps were cured at 120 °C for 12 h for complete cross-linking of the elastomer and to make the patterns permanent. The cured Sylgard 184 films were detached from the stamps after being cooled to room temperature.

For the spin coating of polystyrene (PS), 200 μL of dilute solution of monodispersed PS (MW = 280 000, Sigma, U.K.) in toluene (HPLC grade, SRL Chemicals, India) was dispensed on the substrates

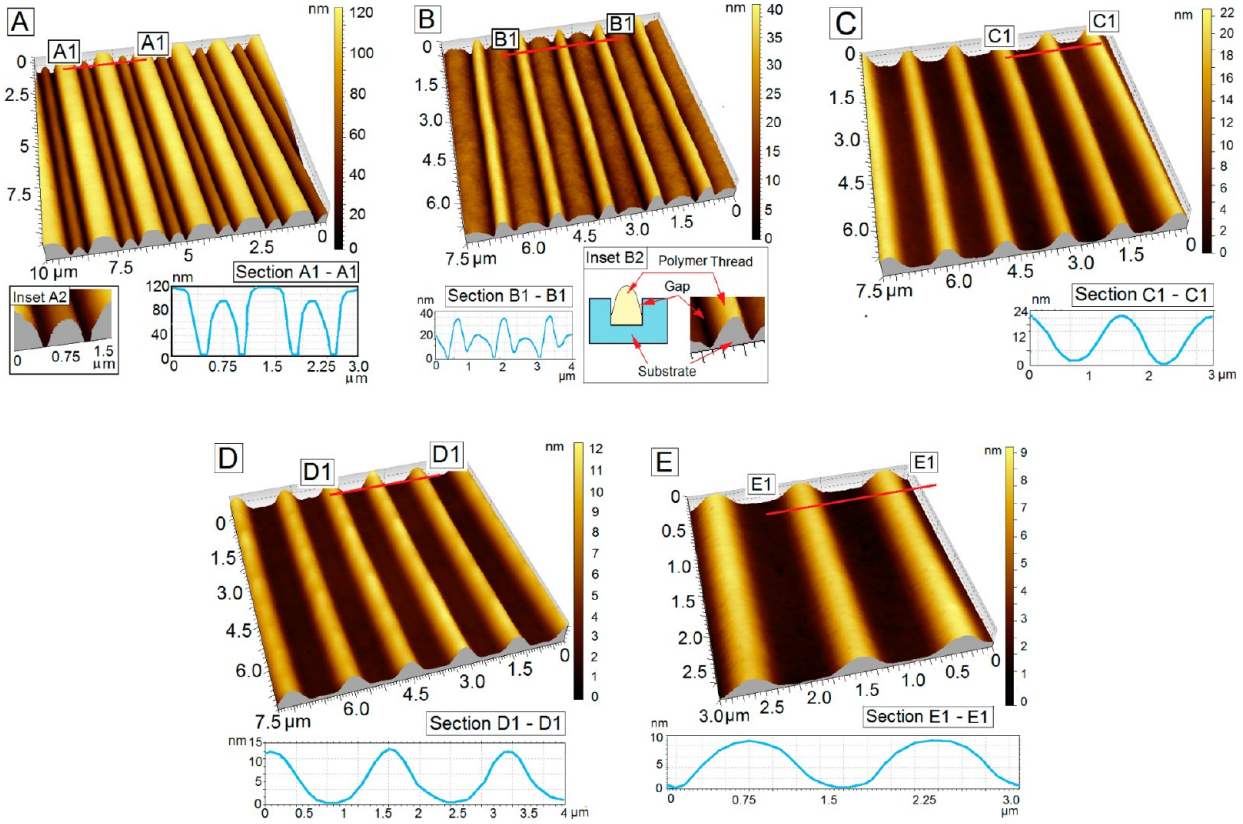

Figure 1. As-cast morphology of a polystyrene (PS) thin film with $\mathbf{h_E}$ = 50.3 nm on substrates with different $\mathbf{H_S}$ values: discontinuous films on (A) $\mathbf{H_{S120}}$ and (B) $\mathbf{H_{S100}}$ substrates and continuous films on (C) $\mathbf{H_{S70}}$, (D) $\mathbf{H_{S40}}$, and (E) $\mathbf{H_{S25}}$ substrates.

and spun at 2500 rpm for 1 min in a spin coater (Apex Instruments, India). After spin coating, the films were annealed in air at room temperature for 1 h and subsequently at 60 °C for 6 h in a vacuum oven to remove any residual solvent. Before dewetting, the as-cast morphology of each film was investigated using atomic force microscopy (AFM). Subsequently, the films were dewetted by annealed at 130 °C for different durations in a vacuum oven. The samples were withdrawn from the oven, cooled to room temperature, and were morphologically characterized using an optical microscope (Leica, DM2500) and an AFM (Agilent Technologies, USA, Model 5100) using intermittent contact mode with a Silicon Cantilever (PPP-NCL, Nanosensors, Inc., USA). Typically, samples were withdrawn after every 30 min to observe the morphological evolution.

For a film coated directly on a topographically patterned substrates, there is no simple way to define a film thickness ($\mathbf{h}$), as the film is either discontinuous or has an undulating top surface.[50,53,54] Therefore, we considered an equivalent film thickness ($\mathbf{h_E}$) for a film coated on a flat surface under identical conditions, the thickness of which was measured using an ellipsometer (Accuron GmbH, Model EP3). While majority of our experiments were performed with films having $\mathbf{h_E}$ = 50.3 ± 1.2 nm (concentration of the PS solution, $\mathbf{c_n}$ = 1.25%, wt/vol) some experiments were also performed with $\mathbf{h_E}$ = 22.1 ± 0.6 nm ($\mathbf{c_n}$ = 0.4%), 62.1 ± 1.9 nm ($\mathbf{c_n}$ = 1.5%), and 80.3 ± 2.2 nm ($\mathbf{c_n}$ = 2.0%) to understand the effect of film thickness variation. The error bars correspond to thickness measurement in at least five films.

One of the key reason for using a cross-linked Sylgard substrate was to economically generate large numbers of patterned substrates by replica molding using limited numbers of lithographically fabricated stamps with different $\mathbf{H_S}$. Secondly, several recent articles on pattern directed dewetting has been performed on topographically patterned Sylgard 184 substrates, arguably due to ease of fabrication.[40−42] Thus, our choice of substrate also allow us to directly compare the findings reported in this article with existing results. One might, at this point, argue that, because toluene is a good solvent for PDMS, there might be a possibility of limited swelling of the Sylgard 184 substrates during spin coating of the PS film. However, we have recently shown that this possibility can be negated as the duration of spinning is very short and the volume of the dispensed solution is low.[50,55,56] Furthermore, although there is a fair deal of difference in the coefficient of thermal expansion between PS and PDMS, our observation revealed that the mismatch in thermal expansion has a very limited influence on dewetting. A short discussion on this issue can be found in the online supporting material.

For each equivalent film thickness−substrate height ($\mathbf{h_E}$−$\mathbf{H_S}$) combination, experiments were repeated at least four times in samples prepared across different batches to verify the reproducibility of the results. The contact angle measurements were also performed at four different locations on each sample. Thus, the error bar corresponds to the average over ∼20 readings for each category of dewetted structure.

RESULTS AND DISCUSSIONS

Morphology of the as-Cast Films on Grating Substrates with Different $\mathbf{H_S}$. We first explore the influence of $\mathbf{H_S}$ on dewetting of PS films with $\mathbf{h_E}$ = 50.3 nm in detail, and then extend our investigations for other film thicknesses to understand the combined influence of $\mathbf{h_E}$ and $\mathbf{H_S}$ on the final pattern morphology.

Figure 1 shows the morphology of the as-cast PS films ($\mathbf{h_E}$ = 50.3 nm) on grating substrates with different $\mathbf{H_S}$. It can be seen that the as-coated films are discontinuous in Figures 1A and 1B, forming isolated polymer threads inside the substrate grooves on the $\mathbf{H_{S120}}$ and $\mathbf{H_{S100}}$ substrates, respectively. The films are continuous with undulating top surfaces in Figures 1C−E, on the $\mathbf{H_{S70}}$, $\mathbf{H_{S40}}$, and $\mathbf{H_{S25}}$ substrates. A continuous film is also observed on $\mathbf{H_{S80}}$, $\mathbf{H_{S60}}$, and $\mathbf{H_{S10}}$ substrates, images of which are not shown. Therefore, it is obvious that the critical $\mathbf{H_S}$ value at which the morphology of the as-cast film changes from continuous to discontinuous lies between 80 nm and 100 nm.

dx.doi.org/10.1021/am301311d | ACS Appl. Mater. Interfaces 2012, 4, 5375−5385

The transition of film morphology from continuous to discontinuous with increasing H_S is in expected lines and complements previously reported observations on direct spin coating of a polymer film on a topographically patterned substrate, where a transition from continuous to discontinuous film has been observed with progressive reduction of the dispensed polymer solution concentration (C_n).[50] We argue that in situ dewetting of the solvent-rich layer during spin coating itself is responsible for the discontinuity of the films on substrates with higher H_S ($\geq$ 100 nm), a detailed mechanism of which is available elsewhere.[50] Figure 1A further reveals that, on a H_{S120} substrate, the confined polymer threads do not span the entire width of the channel. The cross-sectional AFM linescan shows that the width of a single thread is ~600 nm, in contrast to a channel width of 750 nm, which can also be seen in the inset labeled "A2" of the same figure. Furthermore, the height of the polymer strip in this case is ~95 nm, which is lower than the H_S (120 nm) value of the substrate. In contrast, on a H_{S100} substrate, the polymer threads span the entire width of the channels, as seen in Figure 1B. In this case, the thread height is ~112 nm, which is higher than the substrate H_S of 100 nm. The cross-sectional AFM scan further reveals that the polymer thread occupies the entire width of the channels only toward the bottom of the grooves, as the thread boundary is distinct from the contours of the substrate in the upper parts (inset "B2"), which implies that the threads form a contact line with the side walls of the confining stripes and do not impinge on top of the substrate stripes.

For substrates with H_S < 80 nm, the as-cast films are continuous with an undulating top surface. It can be seen that the amplitude of the surface undulations (a_S) reduces with progressive reduction in H_S. Furthermore, since a cross-linked PDMS substrate is partially wetted by the solvent (toluene), the surface undulations are 180° out of phase, with respect to the substrate patterns, which has been shown recently.[50] The schematic in Table 1 shows that the film is thinnest over the substrate stripes, where the local thickness is marked as h_L. We have calculated an approximate value of h_L for each substrate, based on the value of a_S and h_E, which is shown in Table 1. The simplified calculation procedure is documented in the online Supporting Information section. We note that, with reduction of H_S, there is a gradual and significant increase of h_L from ~4 nm on a H_{S80} substrate to ~44 nm on a H_{S10} substrate.

Table 1. Details of the Surface Undulations on as-Cast Films

Substrate Identification	H_S (nm)	a_s (nm)	h_L (nm)	Schematic Representation
H_{S120}	120	--	--	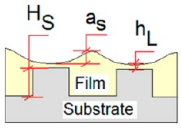
H_{S100}	100	--	--	
H_{S80}	80	26	3.7	
H_{S70}	70	22	9.7	
H_{S60}	60	16	16.2	
H_{S40}	40	12	27.2	
H_{S25}	25	8	35.7	
H_{S10}	10	4	44.2	

In the subsequent sections, we discuss the rupture and dewetting of PS films on different H_S substrates, for films with h_E = 50.3 nm. We first discuss the instability in discontinuous as-cast films, followed by results on dewetting of films with continuous as-cast morphology.

Morphological Evolution and Dewetting of Discontinuous as-Cast Films. On both H_{S120} and H_{S100} substrates (shown in Figures 1A and 1B, respectively), the first signature of instability is observed after 2 h of annealing in the form of regular periodic undulations of alternating narrower and wider regions along each thread, as shown in Figures 2A and 3A, respectively. No undulations are observed before 2 h of annealing. The relatively slower dynamics can be attributed to high molecular weight of the PS used in our experiments. The appearance of the undulations in the confined polymer threads is due to the well-known Rayleigh−Plateau instability, which is engendered by the cross-sectional curvature of the long polymer threads.[57] Rayleigh instability mediated disintegration of polymer filaments supported on a solid substrate is observed in the dewetting of a thin polymer film on a flat substrate as well, in the stage where the cellular polygonal patterns arising out of coalescence of neighboring holes decay into isolated droplets.[2,5−8] The amplitude of the undulations along the axial direction of the threads (seen in Figures 2A and 3A) grow with time, which is associated with a short-range redistribution of liquid from the narrower zones of the undulating thread to neighboring wider zones where a bulge has formed because of the accumulation of polymer. Eventually, the undulating thread snaps off at the narrower locations because of the merging of the advancing polymer/air interfaces from the two sides, resulting in a highly ordered and periodic array of aligned, and nearly equal-sized droplets (Figure 2B), which forms after 5 h of annealing, and does not undergo any subsequent morphological change upon annealing for longer durations. The droplet periodicity along the direction of the stripes (1.13 ± 0.116 μm) corresponds to the λ of Rayleigh instability itself, which is a function of the width of the polymer thread.[55] The final droplets are nearly spherical with a diameter of ~750 nm, which matches the width of the substrate grooves. We also observed that right after detachment of threads (after 4.5 h of annealing), the droplets were slightly elongated as can be seen in the inset labeled "B2" of Figure 2B. The elongated shape is energetically unfavorable, and consequently with time, the droplets acquire a more-symmetric spherical shape, which corresponds to a lower surface energy configuration.

In contrast to aligned droplets obtained on a H_{S120} substrate, the final dewetted morphology on a H_{S100} substrate comprises of periodically undulating polymer threads that bears a clear signature of Rayleigh instability (Figure 3B). The undulated stripes appear roughly after 5 h of annealing, and do not decay or coalesce with time. Although the origin of instability of the polymer thread is same on the H_{S120} and H_{S100} substrates, the difference in the final morphology is attributed to the relative widths of the polymer thread and the substrate groove. It has already been pointed out that the polymer threads do not occupy the entire groove width on a H_{S120} substrate, as compared to a completely filled groove on a H_{S100} substrate. This difference in the initial morphology has a significant influence on the final dewetted patterns. For an undulating thread to decay into droplets, liquid from the thinner zones of the thread needs to physically flow to the thicker, bulgy areas. Since the initial thread does not occupy the entire groove width on a H_{S120} substrate, the liquid can flow out from the narrower zones to the thicker zones, which eventually leads to a breakage of the thread. In contrast, because the entire groove is filled with polymer on a H_{S100} substrate, liquid flow is not possible,

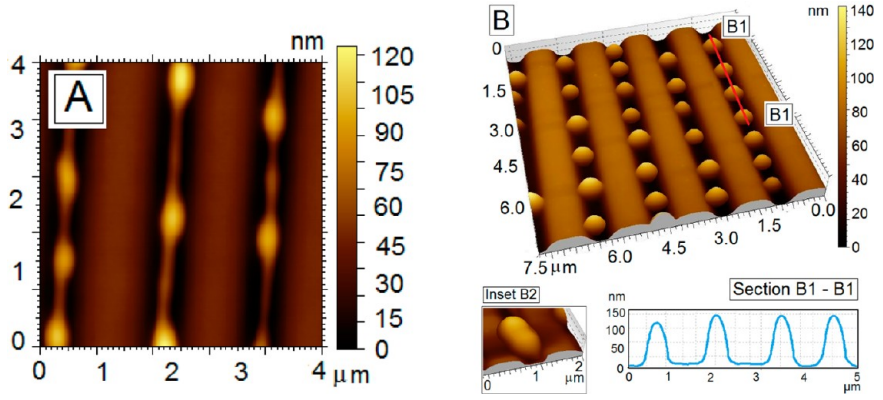

Figure 2. (A) Undulating polymer threads due to Rayleigh instability confined within substrate channels on a $\mathbf{H_{S120}}$ substrate after 2 h of thermal annealing. (B) Final dewetted morphology comprising array of nearly equal-sized aligned droplets after annealing for 5 h. Inset B2 shows initial elongated droplets.

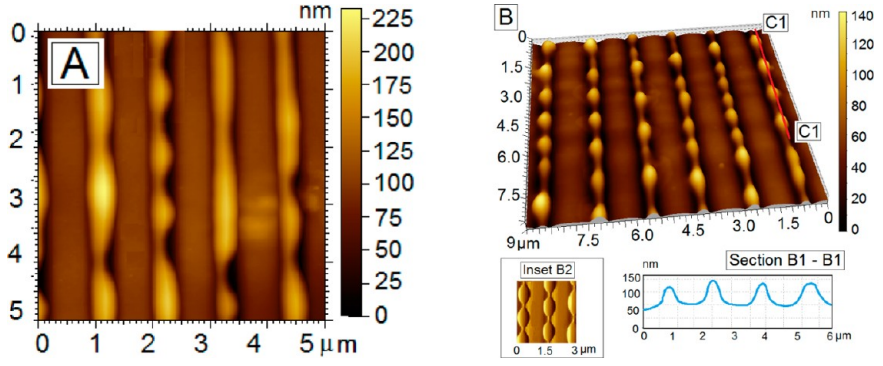

Figure 3. (A) Undulating polymer threads on a $\mathbf{H_{S100}}$ substrate after annealing for 2 h. (B) Final dewetted morphology comprising undulating polymer ribbons aligned along substrate threads, after 5 h of annealing. Inset B2 shows that the ribbons are laterally confined within the substrate grooves and do not impinge on top of the stripes.

which suppresses the subsequent droplet formation cascade. The undulations still appear on the threads as the Rayleigh instability results in redistribution of liquid within the limited gap space available between the thread and the substrate grooves on the upper parts of the grooves, as can be seen in the inset of Figure 1B. Furthermore, no part of the undulating ribbon impinges on the adjoining substrate stripes, and the final pattern remains confined entirely within the grooves, which can be seen in inset B2 of Figure 3B.

Thus, it becomes clear that, for a discontinuous as-cast film morphology on a grating substrate, two distinct final dewetted morphologies are possible, depending on the magnitude of $\mathbf{H_S}$, which, in turn, influences the relative widths of the isolated polymer threads and the substrate groove. We term the aligned array of isolated drops on a $\mathbf{H_{S120}}$ substrate as the *Category 1* structure and the aligned undulating ribbons formed on the $\mathbf{H_{S100}}$ substrate as the *Category 2* structure. Both the structures are perfectly ordered and anisotropic. It is worth pointing out that, while aligned droplet arrays have been observed previously in the dewetting of thin polymer films on grating patterned substrates,[38,40] the occurrence of well-ordered undulating threads previously has never been observed before.

Morphological Evolution and Dewetting of Continuous as-Cast Films. In contrast to discontinuous as-cast films, where the onset of instability is with undulations of the isolated polymer threads, in a continuous film, the dewetting sequence initiates with its rupture, followed by subsequent morphological evolution. On a $\mathbf{H_{S70}}$ substrate, the film is seen to initially rupture between each undulating ridge on the film surface with the formation of tiny holes after 30 min of annealing (Figure 4A). It can be clearly understood, combining Figure 4A with the schematic shown in Table 1, that the film has ruptured over each substrate stripe, where $\mathbf{h_L}$ is the lowest, as the undulations on the film surface are 180° out of phase with the substrate patterns on a partially wettable cross-linked PDMS substrate.[50] A similar rupture sequence is also observed on a $\mathbf{H_{S80}}$ substrate (images not shown), where $\mathbf{h_L}$ is even lower. In both cases, the attractive van der Waals interaction between the film/substrate and film/air interfaces is much stronger over the substrate stripes, compared to other parts of the film, which, in turn, results in a preferential rupture of the film over each stripe, with the formation of holes. Subsequent growth of the holes (inset A2, Figure 4A) leads to retraction of the three-phase contact line (air−substrate−polymer), revealing each substrate stripe top and localizing the polymer in the form of isolated threads, over the substrate grooves, which is seen in Figure 4B. At this stage, the morphology of the ruptured film closely resembles the as-cast film on a $\mathbf{H_{S100}}$ substrate (Figure 1B). Subsequent morphological evolution is due to Rayleigh instability of the isolated polymer threads, which eventually results in a final dewetted morphology comprising undulated aligned ribbons along each substrate groove, as shown in Figure 4C, observed after 4.5 h of annealing. Similar to the situation on a $\mathbf{H_{S100}}$ substrate, in this case, the substrate grooves are completely filled by polymer; and therefore no space is available for the growth of the undulations along the threads. Consequently, the droplet

dx.doi.org/10.1021/am301311d | ACS Appl. Mater. Interfaces 2012, 4, 5375−5385

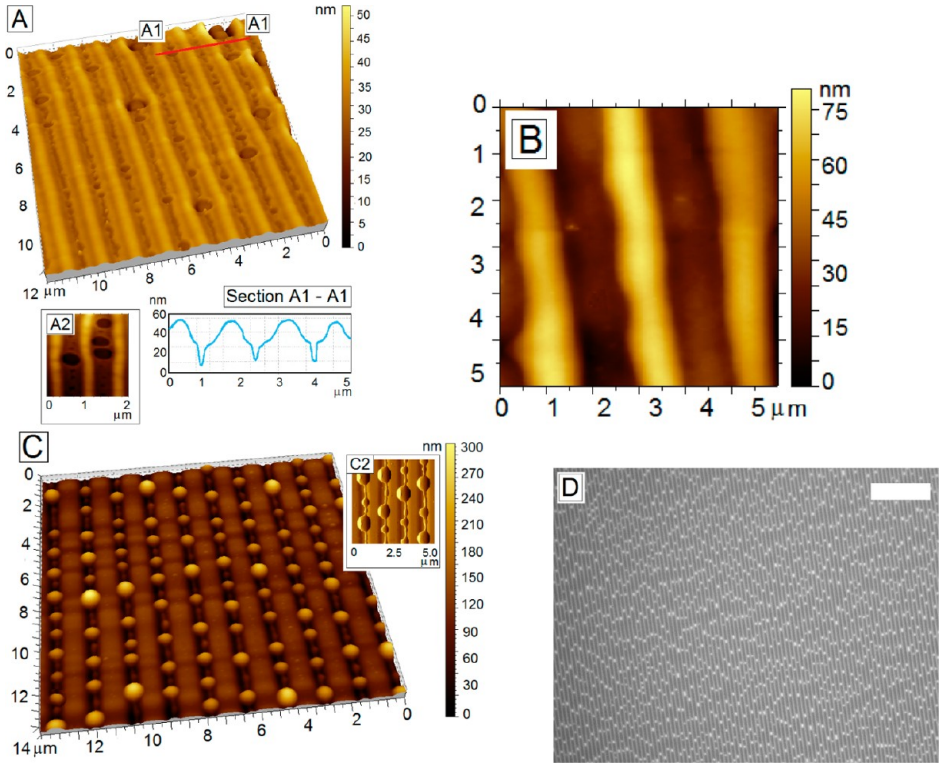

Figure 4. (A) Ruptured film on a H_{S70} substrate, with the appearance of tiny holes along the valleys on the undulating film surface, after annealing for 30 minutes. (B) Isolated ribbons of polymer localized over the substrate grooves due to retraction of the three-phase contact line from areas over the substrate stripes. (C) Undulating polymer ribbons aligned along substrate threads observed after 4.5 h of annealing. Inset C2 confirms that the ribbons do impinge on top of the stripes. (D) Low-magnification optical microscope image showing that the structures span a large area of the substrate.

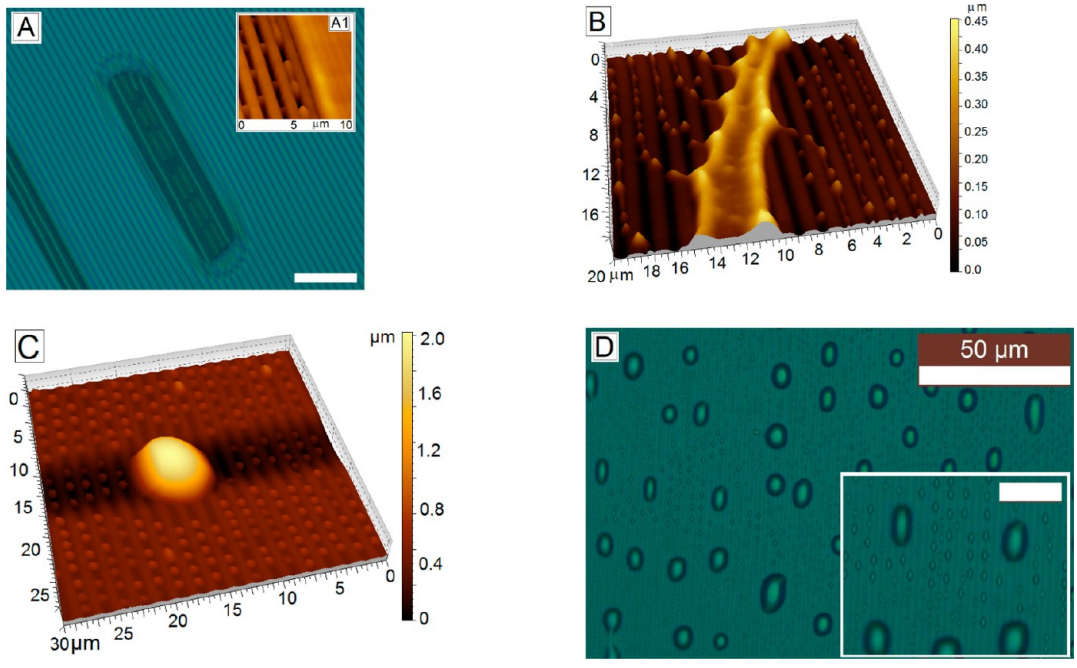

Figure 5. (A) Rupture of a film with the nucleation of anisotropic holes on a H_{S40} substrate. Inset A1 shows undulations on the primary threads detached on the substrate grooves during hole growth. (B) Secondary polymer filament resulting from hole coalescence on a patterned substrate, alongside undulating primary polymer threads. (C) AFM image of the final dewetted morphology comprising a large droplet uncorrelated to the substrate pattern and undulating polymer threads along the substrate grooves. (D) Optical microscope image confirms the uniformity of the morphology over a wide area of the substrate, with the inset showing a high-magnification micrograph, confirming the presence of both structures. Scale bar in inset for panel (D) is 20 μm.

formation is suppressed and the final morphology comprises of aligned, undulating ribbons. However, a careful comparison between Figures 3B and 4C reveals one important difference. On a H_{S70} substrate, the undulations impinge on the substrate

dx.doi.org/10.1021/am301311d | ACS Appl. Mater. Interfaces 2012, 4, 5375−5385

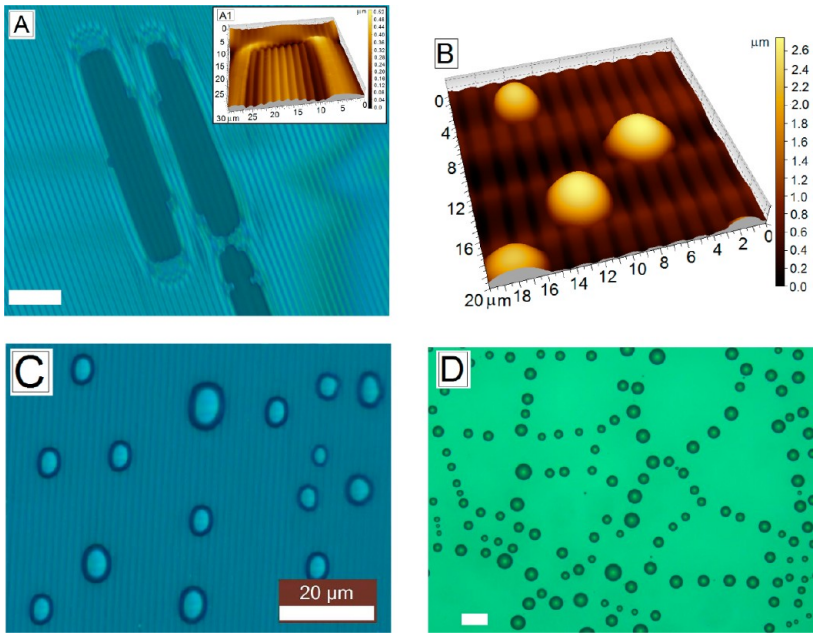

Figure 6. (A) Rupture of a film with the nucleation of anisotropic holes on a H_{S25} substrate. Inset A1 shows an AFM scan of the ruptured hole and confirms that no polymer threads have detached along the substrate grooves. (B) AFM image of the final dewetted morphology, comprised of large dewetted droplets uncorrelated to the substrate pattern, resting on the patterned substrate. (C) Optical microscope image confirms the uniformity of the morphology over a wide area of the substrate. (D) Morphology of a dewetted 42.3-nm-thick film on a flat substrate. Scale bar in panel (D) is 20 μm.

stripe (which can be clearly seen in the inset C2 of Figure 4C), which does not happen on a $\mathbf{H_{S100}}$ substrate. This distinction can be attributed to the fact that, on a $\mathbf{H_{S100}}$ substrate, only the bottom part of the groove is completely filled by the polymer, as the top portion of the thread has a spherical cross section, distinct from the contours of the substrate groove (Figure 1C). Therefore, there was no possibility of any flow of polymer over the substrate stripes, during undulations of the thread, which has already been discussed. In contrast, on the H_{S70} substrate, the threads form due to initial dewetting of the polymer layer on the substrate stripes; therefore, not only are the grooves entirely filled, but the polymer threads form a continuous contact line along the stripes. This allows part of the liquid to overflow onto the top of the stripes, when the thread becomes undulating. Figure 4D is a low-magnification optical microscope image, which shows that these ordered undulated structures span over large areas of the film. Finally, we argue that, despite slight differences in morphology between Figures 4C and 3B, the final dewetted patterns on the $\mathbf{H_{S70}}$ and $\mathbf{H_{S80}}$ substrates are qualitatively similar to that obtained on a $\mathbf{H_{S100}}$ and, therefore, are also classified as *Category 2* structures. Thus, it must be highlighted that *Category 2* is a structure possible in both discontinuous (on $\mathbf{H_{S100}}$ substrate) and continuous (on $\mathbf{H_{S80}}$ and $\mathbf{H_{S70}}$ substrates) as-cast films.

In contrast to the film rupturing over each stripe on $\mathbf{H_{S70}}$ and $\mathbf{H_{S80}}$ substrates, for $\mathbf{H_S} \leq 60$ nm, the film ruptures with the formation of random nucleated holes, in a manner similar to that observed in the dewetting on a flat substrate. With reduced $\mathbf{H_S}$, $\mathbf{h_L}$ increases and, therefore, the difference in the strength of the attractive van der Waals force over the stripes, compared to that over other areas of the film, which was responsible for the preferential rupture of the film on a $\mathbf{H_{S70}}$ substrate, progressively diminishes. A change in the mode of film rupture results in a completely different dewetting pathway of the films on substrates with $\mathbf{H_S} \leq 60$ nm. The holes seen in Figures 5A and 6A on $\mathbf{H_{S40}}$ and $\mathbf{H_{S25}}$ substrates, respectively, appear after ~60 min of thermal annealing. In contrast to customary circular holes on a flat substrate, here, the holes are anisotropic, because their circumference is aligned along the substrate stripes, which is clearly seen in both figures. The anisotropy of the hole shape results due to different rates of retraction of the three-phase contact line, depending on its relative orientation, with respect to substrate geometry. In situ observation shows (a detailed study on the contact line dynamics and rim shape is beyond the scope of this article and will be taken up separately) that the contact line retracts at a much faster rate in the direction of the stripes, in contrast to a significantly slower dynamics in the transverse direction, where the contact line must travel over the substrate stripes, which act as "hurdles". The directional difference in the rates of contact line retraction results in noncircular holes elongated along the direction of the stripes.

Although a slower contact line dynamics in the transverse direction is observed on all substrates with $\mathbf{H_S}$ varying between 10 nm and 60 nm, the effect is more pronounced on $\mathbf{H_{S60}}$ and $\mathbf{H_{S40}}$ substrates, where the contact line is seen to be pinned over each substrate groove for a significant duration of time (a few minutes) before rapidly shifting to the next groove. This shows that the dynamics of the contact line in the transverse direction is of stick slip type, in contrast to a rapid, continuous retraction observed along the direction of the stripes. Furthermore, as the contact line shifts from its current pinning location to the subsequent one, it leaves behind a thread of polymer covering the substrate groove over which it was previously pinned. The detached polymer threads (which, in this context, we term as the "primary threads") can be seen in Figure 5A. Thus, the ruptured part of a hole now is comprised of aligned polymer threads along the substrate grooves and has a morphology that is similar to that observed in Figure 4B. As usual, the isolated threads subsequently start to undulate due to Rayleigh instability, which can be seen in the inset of Figure 5A. Concurrently, the holes

continue to grow with the retraction of the contact line and, eventually, exactly in a manner similar to that observed on a flat substrate, the rims of adjoining holes merge with each other, forming secondary polymer threads. A typical secondary thread is shown in Figure 5B, obtained after 4 h of annealing. It can be clearly seen from the figure that the secondary thread is much wider than the primary threads and spans over several substrate stripes without getting aligned along them. Eventually, the secondary polymer filaments break down into isolated large droplets (again, due to Rayleigh instability), resulting in a final dewetted morphology that is comprised of large drops formed due growth of holes, which are surrounded by undulating polymer threads aligned along the substrate stripes, due to detachment of threads from the retracting polymer meniscus on the patterned substrate. The final dewetted morphology, which is shown in Figure 5C, as well as Figure 5D is obtained after ∼7 h of annealing. While the AFM image in Figure 5C shows, in detail, one large dewetted drop resting on a patterned substrate that contains undulated polymer threads aligned along the substrate grooves, the optical microscope image in Figure 5D shows the coexistence of the two types of structures over the entire sample.

With subsequent reduction in $\mathbf{H_S}$, the resistance offered by the substrate stripes to the retracting contact line gets reduced. It is observed on $\mathbf{H_{S10}}$ and $\mathbf{H_{S25}}$ substrates that the contact line dynamics along the transverse direction over the substrate stripes is much faster, with virtually no pinning on the substrate grooves, compared to that on a $\mathbf{H_{S40}}$ substrate, although the dynamics is still slower than that along the direction of the stripes. In clear contrast to our observation on $\mathbf{H_{S40}}$ and $\mathbf{H_{S60}}$ substrates, virtually no pinning is observed in the present case, because the contact line retracts smoothly over the low feature asperities. In the absence of pinning, no polymer thread is found to detach from the retracting contact line along the substrate grooves over the areas of the film that have ruptured, which can be seen in Figure 6A. The final dewetted morphology in this case comprises of only random large droplets resting on the patterned substrate, which are completely uncorrelated to the substrate stripes, as can be seen in Figure 6B after 4 h of annealing, on a $\mathbf{H_{S25}}$ substrate. The intermediate stages are comprised of the formation of secondary threads only due to rim coalescence (images not shown). The complementary optical microscope image in Figure 6C shows the existence of large droplets over the entire patterned substrate. We observe that, on a $\mathbf{H_{S25}}$ substrate, the final dewetted morphology is attained after ∼4 h of annealing, which is in contrast to ∼7 h taken by the film to fully dewet on a $\mathbf{H_{S40}}$ substrate. The slower dynamics on a higher $\mathbf{H_S}$ substrate is attributed to the stick slip motion of the contact line, because of pinning imparted by the substrate asperities.

Another issue that must be highlighted is that Figure 6C gives an impression that, for low $\mathbf{H_S}$, there is no influence of substrate features on the dewetting pathway or the final dewetted patterns, which are in the form of random droplets, with droplet diameter $\mathbf{d_D} = 2.1 \pm 0.2$ μm and average droplet spacing $\boldsymbol{\lambda_D} = 4.3 \pm 0.9$ μm. In contrast, $\mathbf{d_D} = 12.8 \pm 4.3$ μm and $\boldsymbol{\lambda_D} = 33.8 \pm 4.5$ μm, when a 50.3-nm-thick film is dewetted on a flat, control substrate. This clearly shows that, although a low $\mathbf{H_{S25}}$ substrate fails to impart directionality to the dewetted droplets, the rough surface offers more nucleation sites, which results in rupture of the film at more locations with increased number of holes. As we observe larger numbers of smaller droplets as the final dewetted morphology in Figure 6C, we argue that, on a patterned substrate, a greater number of holes nucleates, compared to that on a flat substrate. This can be attributed to two possible factors: first, the existence of the substrate patterns themselves act as heterogeneous nucleation cites, resulting in more number of holes. However, in that case, it is more logical to argue and expect that the film ruptures along every substrate stripe, which, of course, does not happen! The other plausible reason can be due to the presence of the substrate features, the dynamics of the three-phase contact line becomes slower, particularly in the transverse direction, compared to that on a smooth, flat substrate, which, in turn, allows the time for more holes to nucleate on the intact parts of the film. The presence of a larger number of holes limits their maximum size, which leads to narrower (secondary) threads and, therefore, smaller droplets. Of course, one may consider that the level of residual stresses might also be different in case of a film coated on a patterned substrate, in comparison to a film on a flat substrate.[9] The substrate protrusions may lead to additional degree of chain entanglement during spin coating on a patterned substrate which might lead to higher levels of residual stresses, which might lead to greater nucleation in a continuous film coated on a $\mathbf{H_{S25}}$ substrate. This specific issue needs to be explored in detail in the future.

Based on the morphologies observed in Figures 5D and 6C, we identify two more categories of final dewetted patterns. First, we identify the morphology observed in Figures 6B and 6C, which comprises of only large droplets resting on the patterned substrate as the *Category 4* morphology, which is observed on $\mathbf{H_{S25}}$ and $\mathbf{H_{S10}}$ substrates, for films with $\mathbf{h_E} = 50.3$ nm. We now argue that the final dewetted morphology seen in Figure 5C on $\mathbf{H_{S40}}$ (and also $\mathbf{H_{S60}}$) substrate, which is comprised of random large drops, as well as undulating threads of polymer aligned along the substrate grooves, is essentially a combination of *Category 2* and *Category 4* morphologies, and term it as the *Category 3* morphology. It earmarks a transition from an ordered, pattern directed morphology on higher $\mathbf{H_S}$ substrates to isotropic random structures on lower $\mathbf{H_S}$ substrates.

Influence of Film Thickness on Final Dewetted Morphology. While $\mathbf{h_E}$ was maintained at ∼50.3 nm in a majority of the experiments reported in this article, a limited number of experiments were also carried out with films having $\mathbf{h_E}$ values of 22.1, 62.1, and 80.3 nm as well, to investigate the influence of combined $\mathbf{H_S}$–$\mathbf{h_E}$ topographic pattern directed dewetting. We observe that the final dewetted morphology for all the different $\mathbf{H_S}$–$\mathbf{h_E}$ combination fall into any of the four categories identified in the dewetting of 50.3-nm-thick films. The results of the combined influence of $\mathbf{H_S}$ and $\mathbf{h_E}$ on the final dewetting morphology are represented graphically in Figure 7, in the form of a morphology phase diagram. The figure includes the final morphology resulting from both initially discontinuous and continuous films. It can be clearly seen from the figure that the trend of morphological variation with a progressive reduction in $\mathbf{H_S}$ remains qualitatively similar for each $\mathbf{h_E}$, with a mere change in the magnitude of $\mathbf{H_S}$ cutoff at which final dewetted morphology undergoes a change from one category to the subsequent category. The initial morphology of the as-cast films influence the final dewetted patterns significantly. For example, when $\mathbf{h_E} = 22.1$ nm, a discontinuous as-cast film results on all of the different $\mathbf{H_S}$ substrates, and consequently only *Category 1* (on higher $\mathbf{H_S}$) or *Category 2* (on lower $\mathbf{H_S}$) structures are obtained. Similarly, for films with $\mathbf{h_E} = 80.3$ nm, a continuous film results on all of the substrates. For this particular film thickness, on a $\mathbf{H_{S120}}$ substrate, $\mathbf{h_L}$ is <10 nm, which engenders

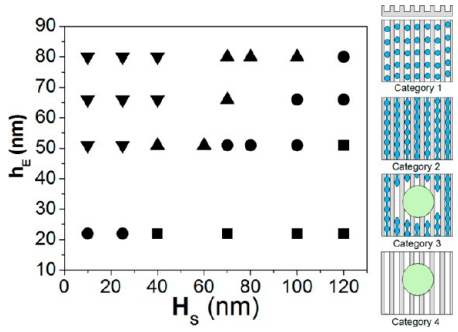

Figure 7. Morphology phase diagram indicating the combined influence of $\mathbf{h_E}$ and $\mathbf{H_S}$ on the final dewetted structures. Legend: (■) *Category 1* morphology, (●) *Category 2* morphology, (▲) *Category 3* morphology, and (▼) *Category 4* morphology. Individual morphologies are schematically shown for ease of understanding.

rupture of the film over each substrate stripe, resulting in *Category 2* structures. In contrast, on substrates with smaller $\mathbf{H_S}$ values, the final morphology varies between *Category 3* and *Category 4*, which is qualitatively identical to that observed for a 50.3-nm-thick film.

Creation of Surfaces with Controlled Wettability Based on the Final Dewetted Morphology. In this section, we discuss a few potential applications of the dewetting mediated patterns formed on topographically patterned substrates with different $\mathbf{H_S}$ values. Our experiments reveal that the different categories of structures with different extent of ordering exhibit different levels of hydrophobicity. More importantly, all the categories of the dewetted structures exhibit higher equilibriums WCA than either the patterned PDMS substrate or a continuous PS film coated on it. For example, the goniometer images in Figures 8A and 8B shows $\boldsymbol{\theta}_{\text{W-PDMS-P}} \approx 105.3^\circ \pm 0.4^\circ$ and $\boldsymbol{\theta}_{\text{W-PS}} \approx 95.2^\circ \pm 0.2^\circ$ on a patterned PDMS substrate with $\mathbf{H_S}$ = 120 nm and on a continuous PS film with $\mathbf{h_E}$ = 50.3 nm coated on that substrate, respectively. A flat cross-linked PDMS substrate exhibits a WCA $\boldsymbol{\theta}_{\text{W-PDMS}} \approx 103.9^\circ \pm 0.3^\circ$. On a shallow patterned substrate, the wetting regime is likely to be Wenzel type.[58] For this wetting regime, the effective equilibrium contact angle ($\boldsymbol{\theta}^*$) is given by the equation

$$\cos \boldsymbol{\theta}^* = \mathbf{r} \cos \boldsymbol{\theta} \qquad (1)$$

where $\mathbf{r}$ is the roughness of the substrate. The equation perfectly validates the variation between $\boldsymbol{\theta}_{\text{W-PDMS-P}}$ ($\boldsymbol{\theta}^*$) and $\boldsymbol{\theta}_{\text{W-PDMS}}$ for $\mathbf{r}$ = 1.16, which is the value of $\mathbf{r}$ on a grating with $\boldsymbol{\lambda}_P$ = 1.5 μm and $\mathbf{H_S}$ = 120 nm. On a dewetted substrate, the values of equilibrium WCA on the different categories of dewetted structures ($\boldsymbol{\theta}_{\text{W-D}}$, shown in Figures 8C−F) vary between 108° and 122° and higher. The highest WCA is observed on a *Category 1* structure, where $\boldsymbol{\theta}_{\text{W-D-Cat1}} \approx 121.8^\circ \pm 0.4^\circ$ (Figure 8C). In order to achieve a WCA of ∼122° on a patterned PDMS substrate, the required level of roughness is $\mathbf{r} \approx 2$, which implies that a grating with $\mathbf{H_S} \approx 750$ nm would be required. Thus, our experiments show that, by using a dewetted film on a grating substrate, it becomes possible to achieve higher level of hydrophobicity, even with shallow substrate features. We argue that the combined influence of topographic roughness, due to the presence of the substrate patterns and the dewetted features, as well as the wettability gradient on the surface between the substrate and the dewetted polymer, is responsible for the manifestation of a higher level of WCA, in comparison to that on both cross-linked PDMS substrate and a continuous PS film. It can further be seen in Figures 8D−F

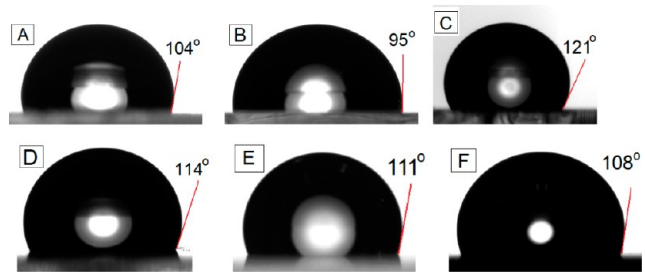

Figure 8. Equilibrium water contact angle (WCA) on a (A) patterned cross-linked PDMS substrate with $\mathbf{H_S}$ = 120 nm, (B) $\mathbf{h_E}$ = 50.3 nm film coated on a $\mathbf{H_{S120}}$ substrate, (C) on a *Category 1* structure, (D) on a *Category 2* structure, (E) on a *Category 3* structure, and (F) on a *Category 4* structure. For panels (C)−(F), $\mathbf{h_E}$ = 50.3 nm.

that the WCA progressively reduces with category of the final dewetted morphology for a $\mathbf{h_E}$ = 50.3 nm film, with $\boldsymbol{\theta}_{\text{W-D-Cat2}} \approx 114.3^\circ \pm 0.6^\circ$ (Figure 8D), $\boldsymbol{\theta}_{\text{W-D-Cat3}} \approx 111.2^\circ \pm 0.2^\circ$ (Figure 8E), and $\boldsymbol{\theta}_{\text{W-D-Cat4}} \approx 107.8^\circ \pm 0.4^\circ$ (Figure 8F), respectively. The progressive reduction in the level of hydrophobicity is attributed to reduced roughness, as well as lower wettability contrast, resulting from larger feature sizes of the dewetted structures. We further observe that the WCA depends rather strongly on the generic category of the final dewetted morphology rather than the precise values of $\mathbf{H_S}$ and $\mathbf{h_E}$. This is verified by the fact that $\boldsymbol{\theta}_{\text{W-D}} \approx 113.9^\circ \pm 0.4^\circ$, $114.9^\circ \pm 0.7^\circ$, and $114.5^\circ \pm 0.5^\circ$ on structures resulting from dewetting of a $\mathbf{h_E}$ = 80.3 nm film on a $\mathbf{H_{S120}}$ substrate, a $\mathbf{h_E}$ = 62.3 nm film on a $\mathbf{H_{S100}}$ substrate and a $\mathbf{h_E}$ = 22.1 nm film on a $\mathbf{H_{S25}}$ substrate, respectively. As can be seen from Figure 7, the final dewetted morphology is *Category 2* in all these cases. Thus, we show that surfaces with controlled wettability can be created by dewetting of a thin polymer film on substrates with different feature heights.

Apart from variation of wettability, dewetting of a thin film on different $\mathbf{H_S}$ substrates has several other potential applications. For example, the *Category 1* patterns can be used for making pixilated display element with optically active luminescent conjugated polymer such as poly(dioctylphenylthiophene) (PDOPT).[33,34] For making pixels, it is important to have isolated features and, therefore, only a *Category 1* structure would suffice. A *Category 1* structure would again be preferred for the potential fabrication of ultrahigh-density magnetic storage and quantum computing applications using binary coordination compounds containing Mn12-based single molecular magnets.[59] In contrast, a *Category 2* structure will be more favorable for dewetting assisted fabrication of organic field-effect transistors.[60] Furthermore, possible fabrication of nanoparticle aggregates by dewetting of a nanoparticle-containing film has already been demonstrated.[2] Based on the concepts presented in this paper, it might become possible to rapidly fabricate dewetting-assisted ordered clusters of metallic nanoparticles. Fabrication of such nanoparticle clusters, which may give rise to new photoluminescence bands in the near-ultraviolet and visible regions typically takes several days by the solid-state route.[61] Thus, the work reported in this paper provides an idea about the necessary initial condition which is likely to lead to a desired morphology, depending on the specific application.

■ CONCLUSION

In this article, we have systematically investigated the influence of substrate feature height ($\mathbf{H_S}$) on dewetting of a thin polymer film on a topographically patterned substrate. We show

that H_S not only influences the final dewetted morphology but also significantly impacts the dewetting mechanism and morphological evolution sequence. We identify four distinct final dewetted morphologies which are possible from the dewetting of a polymer thin film on a grating patterned substrate, which are

Category 1: array of tiny polymer droplets aligned along substrate stripes;
Category 2: aligned undulating polymer threads;
Category 3: a combination of aligned undulating threads and large dewetted droplets; and
Category 4: random collection of large dewetted droplets noncorrelated to the substrate patterns.

Our experiments show that the final dewetted morphology for any h_E−H_S combination falls into any of these categories. For a specific h_E value, the morphology of the final dewetted structures progressively changes from *Category 1* to *Category 4* with a gradual reduction of H_S. The aforementioned morphological transition is also associated with variation in the extent of ordering, as *Category 1* and *Category 2* morphologies comprise perfectly ordered dewetted structures, in contrast to a complete loss of order in *Category 4*. A *Category 3* morphology bears signatures of both pattern-directed and anisotropic dewetting structures and therefore represents a crossover between the two regimes.

We also show that the final morphology of the dewetted patterns are significantly influenced by the initial morphology of the as-coated film on the topographically patterned substrate. The issue that critically influences the subsequent dynamics is whether the as-coated film is discontinuous or continuous. On high H_S substrates, direct spin coating results in discontinuous films with isolated polymer threads aligned along the substrate grooves.[50] Subsequent morphological evolution of such a film can only result in *Category 1* and *Category 2* morphologies, with a *Category 1* morphology being possible only when the polymer threads are narrower than the width of the substrate grooves. Reduction of H_S leads to continuous as-coated films with an undulating top surface, where the undulations on the film surface are 180° out of phase, with respect to the substrate stripes on a partially wettable cross-linked PDMS substrate.[50] In a continuous film, we identify two distinct rupture mechanisms. For low h_L (<10 nm) the film ruptures over each substrate stripe, eventually forming *Category 2* structures. In contrast, when h_L is high (>10 nm) on lower H_S substrates, the film ruptures with the nucleation of random holes, uncorrelated to the substrate patterns in a manner similar to that observed in nucleated dewetting of a film on a flat substrate. Even within the regime where film rupture is nucleation-dominated, we identify two different mechanisms of contact line dynamics during hole growth over the patterned substrate, which significantly impacts the morphology of the final dewetted structures. We observe that a higher H_S substrate offers significant resistance to hole growth, by pinning the three-phase contact line over the substrate grooves. This, in turn, results in a stick slip motion of the contact line, which leaves behind a polymer thread over each substrate groove where it was pinned. The final morphology thus comprises of large dewetted drops resulting from the dynamics of the three-phase contact line during hole growth and tiny undulated polymer threads detached during the stick slip motion of the retracting polymer meniscus, resulting in multi-length-scale *Category 3* structures. On the other hand, substrate stripes with lower H_S fails to pin the retracting polymer meniscus and, therefore, the final dewetted morphology is comprised only of isolated random polymer droplets, resulting in a *Category 4* structure, which is morphologically similar to that observed in the dewetting of a thin film on a flat substrate.

We have also shown that even when the film thickness is varied, the final dewetted morphologies map on to any one of the four identified categories, the results of which are presented in the form of a morphology phase diagram. The diagram might be used as a broad guideline to identify the required film thickness (h_E) on a substrate with a particular H_S, to achieve a specific desired final dewetted morphology, thereby significantly reducing experimental efforts. We would like to highlight that, although the study involved a specific polymer, it is evident that the phenomena reported here is also valid for other polymers. We also feel that the study will help in the design, interpretation, and understanding in creation and rational manipulation of self-organized meso patterns in thin films by pattern-directed dewetting and can be useful in other interfacial phenomena such as self-assembly and adsorption.

Finally, we have also shown that the structures obtained by dewetting on different H_S substrate can be used for fabricating surfaces with controlled wettability, which depends on the generic morphology of the dewetted patterns, rather than the precise magnitude of h_E and H_S. Interestingly, the level of hydrophobicity achieved is higher than the base hydrophobicity exhibited by either the substrate material or the polymer (PS), and it is attributed to a combined influence of topographic and chemical contrast. We have further discussed several potential applications of the work reported in this paper in areas such as fabrication of displays, transistors, nanoparticle clusters, etc.

■ ASSOCIATED CONTENT

Supporting Information

Online Supporting Information has been provided. This material is available free of charge via the Internet at http://pubs.acs.org.

■ AUTHOR INFORMATION

Corresponding Author

*Tel.: +91-3222 283912. E-mail: rabibrata@che.iitkgp.ernet.in.

Notes

The authors declare no competing financial interest.

■ ACKNOWLEDGMENTS

R.M. acknowledges the support of the Department of Science & Technology (DST), New Delhi, India for funding the research under its Nano Mission program (No. SR/NM/NS-63/2010).

■ REFERENCES

(1) Barnes, K., A.; Karim, A.; Douglas, J. F.; Nakatani, A. I.; Gruell, H.; Amis, E. J. *Macromolecules* **2000**, *33*, 4177.
(2) Mukherjee, R.; Das, S.; Das, A.; Sharma, S. K.; Raychaudhuri, A. K.; Sharma, A. *ACS Nano* **2010**, *4*, 3709.
(3) Xie, R.; Karim, A.; Douglas, J. F.; Han, C. C.; Weiss, R. A. *Phys. Rev. Lett.* **1998**, *81*, 1251.
(4) Reiter, G. *Phys. Rev. Lett.* **1992**, *68*, 75.
(5) Sharma, A.; Reiter, G. *J. Colloid Interface Sci.* **1996**, *178*, 383.
(6) Sharma, A.; Khanna, R. *Phys. Rev. Lett.* **1998**, *81*, 3463.
(7) Seemann, R.; Herminghaus, S.; Jacobs, K. *Phys. Rev. Lett.* **2001**, *86*, 5534.
(8) Becker, J; Grün, G.; Seemann, R.; Mantz, H.; Jacobs, K.; Macke, K. R.; Blossey, R. *Nat. Mater.* **2003**, *2*, 59.

(9) Reiter, G; Hamieh, M.; Damman, P.; Sclavons, S.; Gabriele, S.; Vilmin, T.; Raphaël, E. *Nat. Mater.* **2005**, *4*, 754.
(10) Xue, L.; Han, Y. *Prog. Polym. Sci.* **2011**, *36*, 269.
(11) Gentili, D.; Foschi, G.; Valle, F.; Cavallini, M.; Biscarini, F. *Chem. Soc. Rev.* **2012**, *41*, 4430.
(12) An, L.; Li, W.; Nie, Y.; Xie, B.; Li, Z.; Zhang, J.; Yang, B. *J. Colloid Interface Sci.* **2005**, *288*, 503.
(13) Wang, J. Z.; Zheng, Z. H.; Li, H. W.; Huck, W. T. S.; Sirringhaus, H. *Nat. Mater.* **2004**, *3*, 171.
(14) Chabinyc, M. L.; Wong, W. S.; Salleo, A.; Paul, K. E.; Street, R. A. *Appl. Phys. Lett.* **2002**, *81*, 4260.
(15) Rath, S.; Heilig, M.; Port, H.; Wrachtrup, J. *Nano Lett.* **2007**, *7*, 3845.
(16) Kargupta, K.; Sharma, A. *Phys. Rev. Lett.* **2001**, *86*, 4536.
(17) Kargupta, K.; Sharma, A. *Langmuir* **2002**, *18*, 1893.
(18) Kargupta, K.; Sharma, A. *J. Chem. Phys.* **2002**, *116*, 3042.
(19) Kargupta, K.; Sharma, A. *Langmuir* **2003**, *19*, 5153.
(20) Simmons, D.; Chauhan, A. *J. Colloid Interface Sci.* **2006**, *295*, 472.
(21) Bandyopadhyay, D.; Sharma, A. *J. Phys. Chem. C* **2010**, *114*, 2237.
(22) Bandyopadhyay, D.; Sharma, A.; Rastogi, C. *Langmuir* **2008**, *24*, 14048.
(23) Higgins, A. M.; Jones, R. A. L. *Nature* **2000**, *404*, 476.
(24) Zhang, X.; Xie, F.; Tsui, O. K. C. *Polymer* **2005**, *46*, 8416.
(25) Müller-Buschbaum, P.; Bauer, E.; Maurer, E.; Schlögl, K.; Roth, S. V.; Gehrke, R. *Appl. Phys. Lett.* **2006**, *88*, 083114.
(26) Braun, H. G.; Mayer, E. *Thin Solid Films* **1999**, *345*, 222.
(27) Braun, H. G.; Mayer, E. *Macromol. Mater. Eng.* **2000**, *276/277*, 44.
(28) Erhardt, Martin K.; Nuzzo, Ralph G. *J. Phys. Chem. B* **2001**, *105*, 8776−8784.
(29) Sehgal, A.; Ferreiro, V.; Douglas, J. F.; Amis, E. J.; Karim, A. *Langmuir* **2002**, *18*, 7041.
(30) Julthongpiput, D.; Zhang, W.; Douglas, J. F.; Karim, A.; Fasolka, M. J. *Soft Matter* **2007**, *3*, 613.
(31) Zhang, Z.; Wang, Z.; Xing, R.; Han, Y. *Polymer* **2003**, *44*, 3737.
(32) Zhang, Z.; Wang, Z.; Xing, R.; Han, Y. *Surf. Sci.* **2003**, *539*, 129.
(33) Wang, X.; Ostblom, M.; Johansson, T.; Inganas, O. *Thin Solid Films* **2004**, *449*, 125.
(34) Wang, X.; Tvingstedt, K.; Inganas, O. *Nanotechnology* **2005**, *16*, 437.
(35) Li, W.; Nie, Y.; Zhang, J.; Zhu, D.; Li, X.; Sun, H.; Yu, K.; Yang, B. *Macromol. Chem. Phys.* **2008**, *209*, 247.
(36) Rhese, N.; Wang, C.; Hund, M.; Geoghegan, M.; Magerle, R.; Krausch, G. *Eur. Phys. J. E* **2001**, *4*, 69.
(37) Geoghegan, M.; Wang, C.; Rhese, N.; Magerle, R.; Krausch, G. *J. Phys.: Condens. Matter* **2005**, *17*, S389.
(38) Luo, C.; Xing, R.; Zhang, Z.; Fu, J.; Han, Y. *J. Colloid Interface Sci.* **2004**, *269*, 158.
(39) Khare, K.; Brinkmann, M.; Law, B. M.; Gurevich, E. L.; Herminghaus, S.; Seemann, R. *Langmuir* **2007**, *23*, 12138.
(40) Mukherjee, R.; Gonuguntla, M.; Sharma, A. *J. Nanosci. Nanotechnol.* **2007**, *7*, 2069.
(41) Xing, R.; Luo, C.; Wang, Z.; Han, Y. *Polymer* **2007**, *48*, 3574.
(42) Mukherjee, R.; Bandyopadhyay, D.; Sharma, A. *Soft Matter* **2008**, *4*, 2086.
(43) Yoon, B.; Acharya, H.; Lee, G.; Kim, H. C.; Huh, J.; Park, C. *Soft Matter* **2008**, *4*, 1467.
(44) Suh, K. Y.; Lee, H. H. *J. Chem. Phys.* **2001**, *115*, 8204.
(45) Suh, K. Y.; Park, J.; Lee, H. H. *J. Chem. Phys.* **2002**, *116*, 7714.
(46) Harkema, S.; Schaffer, E.; Morariu, M. D.; Steiner, U. *Langmuir* **2003**, *19*, 9714.
(47) Luo, C.; Xing, R.; Han, Y. *Surf. Sci.* **2004**, *552*, 139.
(48) Kim, Y. S.; Lee, H. H. *Adv. Mater.* **2003**, *15*, 332.
(49) Suh, K. Y.; Lee, H. H. *Adv. Funct. Mater.* **2002**, *12*, 405.
(50) Roy, S.; Ansari, K. J.; Jampa, S. S. K.; Vutukuri, P.; Mukherjee, R. *ACS Appl. Mater. Interfaces* **2012**, *4*, 1887.
(51) Ferrell, N.; Hansford, D. *Macromol. Rapid Commun.* **2007**, *28*, 966.
(52) Mukherjee, R.; Sharma, A.; Gonuguntla, M.; Patil, G. K. *J. Nanosci. Nanotechnol.* **2008**, *8*, 3406.
(53) Mukherjee, R.; Pangule, R. C.; Sharma, A.; Banerjee, I. *J. Chem. Phys.* **2007**, *127*, 064703.
(54) Deb Roy, R.; Sil, D.; Jana, S.; Bhandaru, N.; Bhadra, S. K.; Biswas, P. K.; Mukherjee, R. *Ind. Eng. Chem. Res.* **2012**, *51*, 9546.
(55) Mukherjee, R.; Sharma, A. *ACS Appl. Mater. Interfaces* **2012**, *4*, 355.
(56) Mukherjee, R.; Pangule, R.; Sharma, A.; Tomar, G. *Adv. Funct. Mater.* **2007**, *17*, 2356.
(57) Rayleigh, L. *Proc. London Math. Soc.* **1878**, *10*, 4.
(58) Wenzel, R. N. *Ind. Eng. Chem. Res.* **1936**, *28*, 988.
(59) Cavallini, M.; Gomez-Segura, J.; Albonetti, C.; Ruiz-Molina, D.; Veciana, J.; Biscarini, F. *J. Phys. Chem. B* **2006**, *110*, 11607.
(60) Tong, Y. H.; Tang, Q. X.; Lemke, H. T.; Moth-Poulsen, K.; Westerlund, F.; Hammershoj, P.; Bechgaard, K.; Hu, W. P.; Bjornholm, T. *Langmuir* **2010**, *26*, 1130.
(61) Chattopadhyay, S.; Mukherjee, R.; Datta, A.; Saha, A.; Sharma, A.; Kulkarni, G. U. *J. Nanosci. Nanotechnol.* **2009**, *9*, 190.